ACS APPLIED MATERIALS & INTERFACES

Research Article

www.acsami.org

High-Performance Plastic Dye-sensitized Solar Cells Based on Low-Cost Commercial P25 TiO_2 and Organic Dye

Xiong Yin,[†,‡] Zhaosheng Xue,[†] Long Wang,[†] Yueming Cheng,[†] and Bin Liu*[,†]

[†]Department of Chemical and Biomolecular Engineering, National University of Singapore, Singapore 117576,
[‡]National Center for Nanoscience and Technology, P.R. China

Supporting Information

ABSTRACT: High-performance plastic dye-sensitized solar cells (DSCs) based on low-cost commercial Degussa P25 TiO_2 and organic indoline dye D149 have been fabricated using electrophoretic deposition (EPD) with compression post-treatment at room temperature. The pressed EPD electrode outperformed the sintered EPD electrode and as-prepared EPD electrode in short-circuit current density and power conversion efficiency. About 150% and 180% enhancement in power conversion efficiency have been achieved in DSC devices with sintering and compression post-treatment as compared to the as-prepared electrode, respectively. Several characterizations including intensity modulated photocurrent spectroscopy, incident photon-to-electron conversion efficiency and electrochemical impedance spectra have been employed to reveal the nature of improvement with post-treatment. Experimental results indicate that the sintering and compression post-treatment are beneficial to improve the electron transport and thus lead to the enhancement of photocurrent and power conversion efficiency. In addition, the compression post-treatment is more efficient than sintering post-treatment in improving interparticle connection in the as-prepared EPD electrode. Under optimized conditions, the conversion efficiency of plastic devices with D149-sensitized P25 TiO_2 photoanode has reached 5.76% under illumination of AM 1.5G (100 mW cm^{-2}). This study demonstrates that the EPD combined with compression post-treatment provides a way to fabricate highly efficient plastic photovoltaic devices.

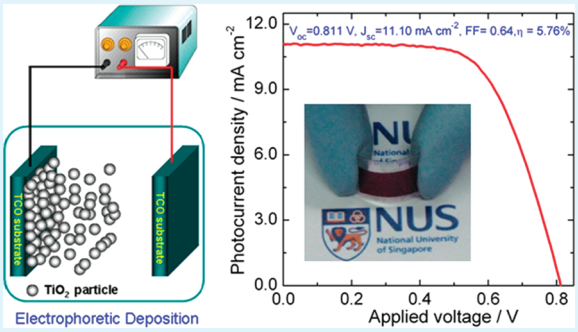

KEYWORDS: *flexible dye-sensitized solar cells, low-temperature fabrication, intensity-modulated photocurrent spectroscopy, electrophoretic deposition, organic dye, P25 TiO_2*

1. INTRODUCTION

Dye-sensitized solar cells (DSCs) have attracted worldwide attention as a new generation of photovoltaic devices with advantages of simple fabrication, low-cost production, and relatively high energy conversion efficiency.[1−3] A typical DSC consists of a dye-sensitized semiconductor photoanode, electrolyte, and a counter electrode. Extensive research efforts have been devoted to developing each component to improve the power conversion efficiency, including highly efficient dye,[3−5] new structure photoanode,[6,7] and low-price counter electrode materials.[8,9] Up to now, DSCs based on nanoporous TiO_2 electrode on rigid glass substrate with zinc porphyrine dye as the sensitizer have shown the conversion efficiency of over 12%.[3] The fabrication steps for photoanodes in these high efficiency DSCs generally require a 450 °C sintering process,[1−3,10] which is not suitable for plastic DSCs as the substrate can only sustain temperature up to 150 °C.[11] Therefore, several strategies have been proposed to fabricate plastic DSCs using different techniques, such as, low temperature hydrothermal synthesis,[12,13] transferring,[14] UV−vis light treatment,[15] binder-free coating,[16] chemical sintering,[17] and spray deposition.[18]

Electrophoretic deposition (EPD) is a widely used method to produce thin films at room temperature.[19] Our previous studies have shown that EPD could be used to fabricate both photoanode and counter electrode for DSCs.[20] In a typical EPD process, particles to be deposited are suspended in a solvent to form a stable colloid. A pair of electrodes will be inserted and a potential difference is applied. Films are formed when charged particles are deposited on the electrodes via electrostatic attraction. However, films prepared by this way generally require post-treatment as they tend to be mechanically unstable compared to sintered films made from pastes with binders. To improve the mechanical stability, interparticle adhesion and electrical connectivity, high temperature sintering is commonly applied. Though convenient, this cannot be applied to flexible plastic substrates. Other than conventional sintering, compression is a low-temperature method that is suitable for flexible substrates and convenient for large scale production.

Received: December 27, 2011
Accepted: February 10, 2012
Published: February 10, 2012

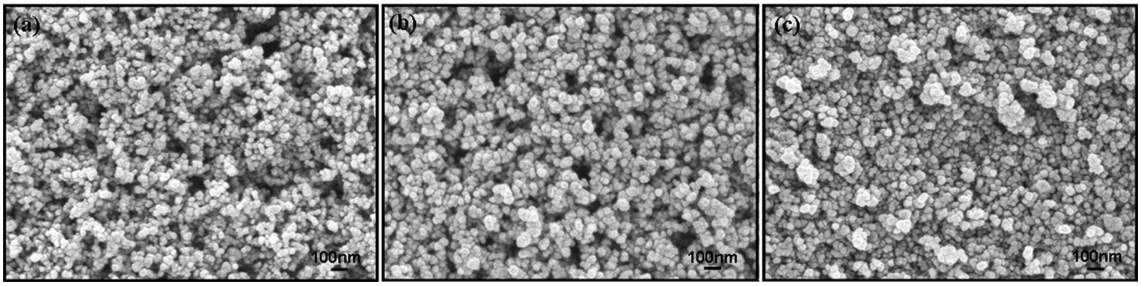

Figure 1. FESEM images of the electrophoretically deposited films: (a) as-prepared; (b) sintered film; (c) pressed film.

Mass production of DSCs requires methods that can be scaled up readily and materials that are available in large quantities. In this regard, using EPD as film fabrication method and commercially available P25 TiO_2 nanoparticles as photoanode material fit the criteria ideally. In addition, this combination is suitable for flexible plastic substrates which have the potential to be used for classic roll to roll mass production. Flexible DSCs based on P25 TiO_2 and inorganic Ru(II) dye N719 presented a conversion efficiency of 4.4% under 1 sun illumination.[21] The conversion efficiency of the plastic devices, sensitized with inorganic Ru (II) dye N3, can be improved from 5.1% to 6.2% via deposition of a double shell amorphous TiO_2/MgO coating on the TiO_2 layer using the sol−gel EPD method.[19]

In this contribution, we report the fabrication of high-performance plastic DSCs based on low-cost P25 TiO_2 and organic indoline dye D149 using EPD combined with compression post-treatment. D149 dye is selected as the sensitizer because it has a large light absorption coefficient, with high power conversion efficiencies in traditional DSCs and it can be easily synthesized with a large quantity.[5a,22] We show that the combination of EPD, P25 TiO_2 and D149 dye can yield a high efficiency of 5.76% for plastic DSCs. In addition, we find that the compression post-treatment is more effective in improving the photoanode quality and the device efficiency as compared to the more commonly used sintering post-treatment for devices fabricated via EPD.

2. EXPERIMENTAL SECTION

2.1. Fabrication of EPD Electrode. The TiO_2 suspension for EPD was prepared by mixing 0.35 g of TiO_2 powder with 10 mL of a mixture of ethanol, isopropanol and butanol (v/v/v = 1:2:4), which was followed by ultrasonication for 30 min. A pair of FTO glass substrates (2 cm ×2.5 cm, 15 Ω sq^{-1}, Hartford) or plastic PEN-ITO substrates (Kintec) was vertically immersed in the suspension and then a 1.6 V cm^{-1} DC field was applied. Because TiO_2 acquired an excessive positive surface charge in the suspension, the P25 TiO_2 particles were successfully deposited on the cathode. Then the as-prepared TiO_2 electrode was heated at 85 °C for 2 h to remove the organic solvents. After drying, the as-prepared TiO_2 electrode was pressed at 1 Ton cm^{-2} for 2 min to yield pressed EPD electrode using a manual hydraulic Press (Atlas) at room temperature. For comparison, the as-prepared electrode was also heated at 450 °C for 30 min to obtain the sintered EPD electrode. For bilayer films, the same EPD procedure was repeated, which was followed by deposition of 400 nm TiO_2 (anatase, Aldrich) atop of the P25 TiO_2 film, and the 400 nm TiO_2 layer is employed as the scattering layer in the DSC devices. After pressed at 1 Ton cm^{-2} for 2 min, the bilayer films were applied to fabricate devices. The dye loading for each electrode with a certain area was obtained by desorbing the electrodes into 0.1 M ammonia in DMSO solution.

2.2. Device Fabrication. After being heated at 85 °C for 1 h, the electrodes were immersed into a 0.5 mM D149 dye solution in a mixed solvent of acetonitrile and tert-butylalcohol (V/V = 1:1) at room temperature for 1 h to sensitize with dye D149. Dye-sensitized electrodes were rinsed with pure acetonitrile and dried under nitrogen flow. The rigid Pt counter electrode was prepared by spin-coating a 5 mM H_2PtCl_6 solution on a FTO glass substrate, followed by sintering at 390 °C for 30 min. The flexible counter electrodes were fabricated by sputtering Pt on the PEN-ITO substrate using a sputtering machine (JEOL, JFM 1100, Japan).

A 25 μm thick hot-melt film (Solaronix) was sandwiched between the TiO_2 photoanode and rigid or plastic Pt counter electrode. The space between the two electrodes was filled with liquid electrolyte. The electrolyte composition was 0.5 M tetrabutylammonium iodide, 0.001 M $LiClO_4$, 0.5 M 4-tert-butylpyridine, and 0.1 M I_2 in 3-methyoxypropionitrile.[20a] The devices masked with a steel mask had an active area of 0.158 cm^2 during characterization.

2.3. Characterization. The morphology of TiO_2 electrodes was observed using a field emission scanning electron microscopy (FESEM, JEOL). The thickness of TiO_2 films was examined by a profilometer (Tencor Alpha-step 500). The particle surface area was determined by N_2 adsorption/desorption studies (NOVA 4200e). The Brunauer−Emmett−Teller (BET) method was used to estimate the specific surface area. Data reported are averages of three samples.

The photovoltaic parameters of DSCs were performed by an AutoLAB PGSTAT 320N Potentiostat with simulator light (AM1.5 100 mW cm^{-2}, San-EI Electric). The incident photon-to-electron conversion efficiency (IPCE) was measured using a 300W Xe light source (MAX-310, Asahi Spectra), a Keithley model 2400 unit and monochromator (TMS 300, Bentham). The intensity-modulated photocurrent spectroscopy (IMPS) were carried out with an Autolab electrochemical workstation (PGSTA320N) and a green light emitting diode (λ = 530 nm). The electrochemical impedance spectroscopy (EIS) of the DSCs was recorded over a frequency range between 0.01 Hz and 1×10^5 Hz under illumination of 100 mW cm^{-2} with the same AutoLab workstation. The applied bias voltage and AC amplitude were set at the open-circuit voltage of the DSCs and 10 mV, respectively. The EIS spectra were analyzed using an equivalent circuit model.[23,24]

3. RESULTS AND DISCUSSION

The FESEM images of the as-prepared EPD electrode, the sintered EPD electrode and the pressed EPD electrode are shown in Figure.1. Individual TiO_2 nanoparticles are clearly observed in the as-prepared electrode (Figure 1a). It is known that freshly prepared EPD films are not mechanically very stable as they suffer weak bonding between the substrate and films.[25] To enhance interparticle connection, the electrode was commonly treated with sintering.[25] Accordingly, some welded nanoparticles with other individual nanoparticles are observed in the sintered EPD electrode (Figure 1b). On the other hand, after pressing, welded TiO_2 particles are also found in the pressed EPD electrode (Figure 1c). It is reasonable that the compression increased the contact area among TiO_2 nanoparticles and strengthened their connection and consequently these welded particles were formed.[26] It can be found in Figure 1 that the sintering post-treatment does not appear to decrease

the cavities in the film, whereas the compression post-treatment apparently does. These results clearly demonstrate that the local geometry of the as-prepared EPD TiO_2 electrode can be easily changed by post-treatment, especially by compression. The effect of post-treatment on the phase composition and the crystallite size of P25 TiO_2 was determined using XRD analysis. The typical XRD pattern of the three electrodes is shown in Figure S1 (see the Supporting Information). The three samples show the similar XRD patterns. The amount of anatase and rutile phases contained in each electrode is calculated by taking the ratio of the two most intense peaks of the anatase $I_A(101)$ and rutile I_R (110). The three electrodes present the same phase composition containing about 80% anatase and 20% rutile, and the crystallite size of particle is about 27 nm calculated using Scherrer's formula. These results indicate that the phase composition and the crystallite size of the P25 TiO_2 powder used in the experiment did not change with the two post-treatments, sintering at 450 °C for 30 min and compression at 1.0 Ton cm^{-2} for 2 min.

The three kinds of TiO_2 electrodes were also examined with the nitrogen adsorption−desorption analysis in order to compare the effect of the post-treatment on the film microstructure. The measurements were carried out on powder which was carefully scratched from the electrodes. The nitrogen adsorption−desorption isotherms for the different electrodes are presented in the Figure 2. The shape of the isotherms is typical for mesoporous materials. According to the Brunauer−Deming−Deming and Teller (BDDT) classification,[27,28] all the samples display a type IV isotherm with a type H3 hysteresis loop. The corresponding pore-size distributions obtained via BJH model applied to the adsorption branch are shown in the inset of Figure 2, which indicates that the pore size of the three different electrodes is in the range from 2 to 30 nm with a rather broad size distribution. This also implies that mesoporosity of the as-deposited EPD TiO_2 film is not lost even after sintering or compression post-treatment. It can be found from Figure 2 that the isotherms of the as-prepared film and the sintered film are almost the same, which indicates that the sintering post-treatment did not have any significant effect on the surface area and pore volume of the films. Meanwhile, from the intersection of adsorption and desorption curves, the monolayer relative pressure for the completion of monolayer adsorption can be determined. The monolayer adsorption for the pressed EPD TiO_2 film is completed at a relative pressure of about 0.24. However, the monolayer adsorption for the as-prepared film and sintered film is not completed until it reaches a relative pressure of about 0.28. This implies that the pressed EPD TiO_2 film possesses much smaller pore size than that in the as-prepared EPD TiO_2 film and sintered TiO_2 film. The Brunauer, Emmett, and Teller (BET) specific surface areas of as-deposited, sintered, and pressed film were 36.5, 38.7, and 42.6 $m^2\ g^{-1}$, respectively, with pore volumes of 0.17, 0.179, and 0.233 $cm^3\ g^{-1}$.

The as-prepared, sintered, and pressed TiO_2 films with thickness of about 13.5, 13.5, and 7.2 μm, respectively, were consequently examined as photoanodes in DSCs after sensitized with dye D149. Figure 3 shows the corresponding photovoltaic curves under illumination of simulated AM 1.5G solar light (100 mW cm^{-2}). In the case of DSC with as-prepared electrode, the short-circuit current density (J_{sc}), open-circuit photovoltage (V_{oc}) and fill factor (FF) values are 3.82 mA cm^{-2}, 0.777 V, and 0.69, respectively, with an overall power conversion efficiency (η) of 2.05%. The DSC based on sintered

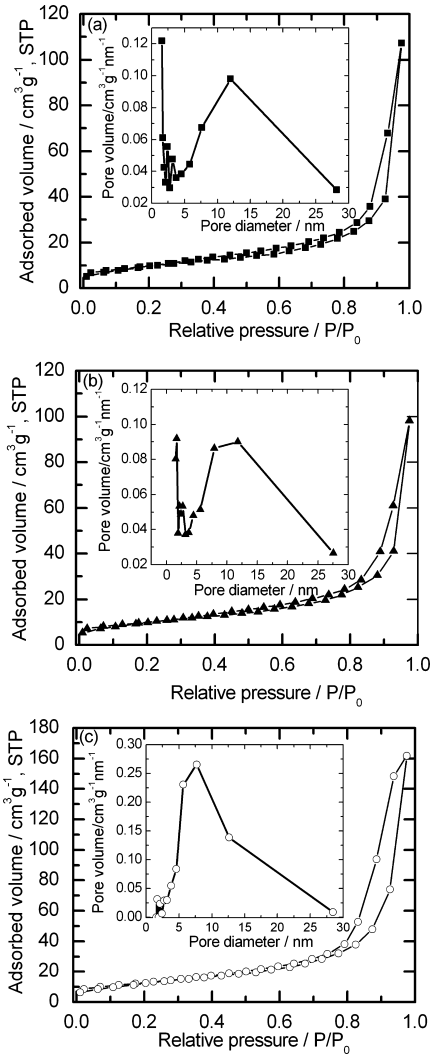

Figure 2. Nitrogen adsorption−desorption isotherms of the films: (a) as-prepared film; (b) sintered film; and (c) pressed film; inset shows the corresponding pore size distribution.

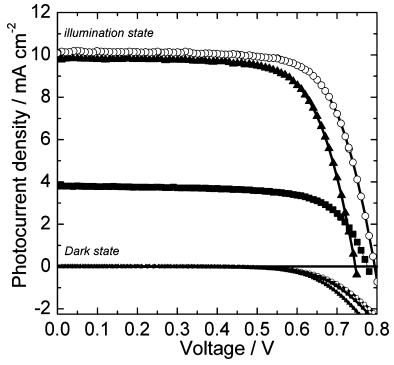

Figure 3. Current density−voltage characteristics curves measured under illumination of 100 mW cm^{-2}, AM1.5G and in the dark of D149-sensitized P25 TiO_2 solar cells with the as-prepared photoanodes (solid squares), the sintered photoanodes (solid triangles) and the pressed photoanodes (open circles).

TiO_2 electrode exhibits a J_{sc} of 9.83 mA cm^{-2}, V_{oc} of 0.745 V and FF of 0.71 yielding η of 5.20%. The corresponding parameters (J_{sc}, V_{oc}, FF and η) of the pressed electrode-based device are 0.795 V, 10.13 mA cm^{-2}, 0.722, and 5.81%,

respectively. The observed results indicate that post-treatments have an obvious effect on the J_{sc} and consequently on the power conversion efficiency. The J_{sc} of the sintered electrode and pressed electrode is about 2.6 and 2.9 times higher than that in the as-prepared electrode, respectively. However, the dye loading for the as-prepared, sintered and pressed TiO_2 films was 1.38×10^{-7} mol cm^{-2}, 1.45×10^{-7} mol cm^{-2} and 8.62×10^{-8} mol cm^{-2}, respectively. Therefore, the improvement in J_{sc} did not stem from the change in dye loading. The reasons for increase in J_{sc} and photovoltaic performance of device after post-treatments will be discussed in detail in the following sections. The difference in power conversion efficiency with two kinds of post-treatment lies mainly in the change of V_{oc} of the devices. To compare the difference in the V_{oc}, we examined changes in the dark current with the applied potential, which is also shown in Figure 3. The dark current is correlated to the recombination of electrons with redox mediator in the electrolyte. The onset of dark current took place at a higher potential for pressed electrode compared to the sintered electrode, implying that the dark current is low for the pressed electrode. The presence of fewer traps due to reduction of film thickness in the pressed electrode should decrease the charge leakage in the pressed electrode. The low recombination reaction would lead to increase in the electron density of the TiO_2 film, which provokes an enhancement in the resulting open-circuit photovoltage. As a result, the decrease of dark current can result in the increase of V_{oc}.[29,30] Therefore, as for the as-prepared electrode via EPD, the compression is an efficient post-treatment to improve the conversion efficiency of device at room temperature. The dependency of photovoltaic properties on the compression pressure was also performed. As shown in the Figure S2 and Table S1 (see the Supporting Information), the J_{sc} and power conversion efficiency reached the maximum value at the pressure of 1.0 Ton cm^{-2}. Then J_{sc} decreased to 9.19 mA cm^{-2} at the pressure of 1.2 Ton cm^{-2}, with the corresponding power conversion efficiency of 5.17%. And the decline is due to a large decrease of dye loading in the film.

To understand the reasons behind the improvement of the device performance after post-treatment, we characterized the devices using intensity-modulated photocurrent spectroscopy (IMPS), incident-photon-to-electron conversion efficiency (IPCE), and electrochemical impedance spectroscopy (EIS).

IMPS was conducted to understand the difference in terms of electron transport among the three photoanodes.[31,32] The typical IMPS plots for three TiO_2 photoanodes are shown in Figure.4a. The intensity of the IMPS shows that the device with pressed electrode presented the largest light response among the three devices in the measured frequency response, which is in good agreement with the measured J_{sc}. The electron transport is evaluated in terms of the electron transport time (τ_d), which is defined as the typical time taken from photoelectron injection to photoelectron arrival at substrate. τ_d can be calculated according to the equation: $\tau_d = (2\pi f_{min})^{-1}$.[33] τ_d for the as-prepared electrode, the sintered electrode, and the pressed electrode were 1.1, 0.43, and 0.37 ms, respectively. This shows that electron transport in the film has been improved after post-treatment. The faster electron transport can lead to the increase in J_{sc} of DSC devices.[32,33]

Figure.4b shows the IPCE spectra of devices with three photoanodes as a function of wavelength. IPCE spectra reflect the light response of photovoltaic devices, which is directly

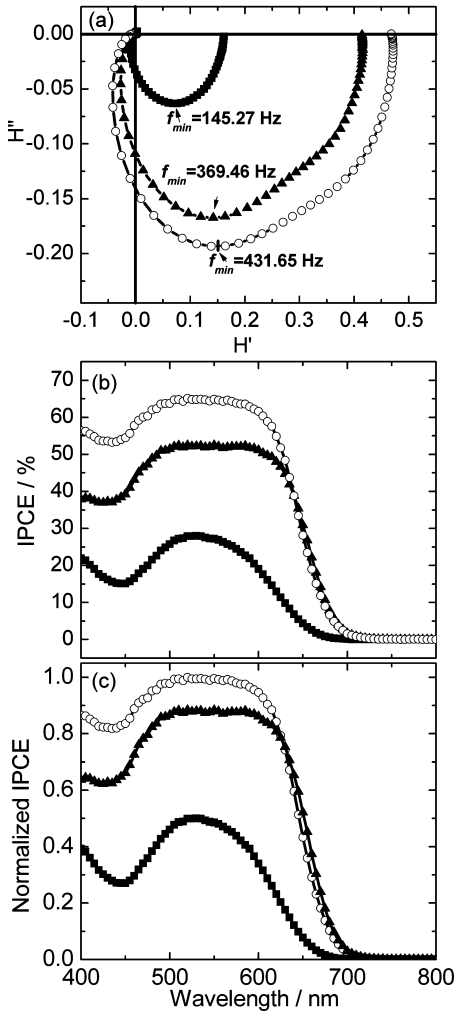

Figure 4. (a) IMPS plots and (b) IPCE spectra and (c) normalized IPCE spectra for DSCs with the as-prepared photoanodes (solid squares), the sintered photoanodes (solid triangles) and the pressed photoanodes (open circles).

related to photocurrent density and can be calculated from the equation[34]

$$\text{IPCE}\ (\%) = 1240 I_{sc}/(\lambda P_{in})$$

Where I_{sc} is the short-circuit photocurrent density at a single wavelength, λ is the wavelength of the incident light, and P_{in} is the power of the incident light.

The devices made of the electrodes with post-treatment possess higher IPCE values than that for the as-prepared in the full range of 400 to 800 nm. The maximum IPCE values for DSCs with the sintered electrode and the pressed electrode are ~85% and 130% larger than that with the as-prepared electrode, respectively. It is well-known that the IPCE is determined by light harvesting efficiency of the dye (LHE), the quantum yield of charge injection (φ_{inj}) and the efficiency of charge collection (η_{cc}) at conducting substrate as shown in equation.[34]

$$\text{IPCE} = \text{LHE}(\lambda)\phi_{inj}\eta_{cc}$$

In our study, the LHE (λ) is mainly proportional to the adsorbed dye molecules per square centimeter. Hence, we used the dye loading to normalize the IPCE spectra, and it is shown in Figure 4c. It is found that the device with post-treatment still

possessed higher IPCE values than that for as-prepared electrode. The large increase in IPCE after post-treatment is dependent on the η_{cc} because the charge injection efficiency from D149 dye to TiO_2 is near unity.[5a] As such, the improvement in η_{cc} with post treatment is manly attributed to good interparticle connections with increase in the contact area among particles and the adhesion strength between the particles and substrate.[35] This study shows that, whereas the as-prepared EPD films are mediocre in device performance, they can be improved easily by applying simple post-treatment steps. In addition, the increase in IPCE is in good agreement with the enhancement of J_{sc} in the devices.

EIS is a powerful technique to study the electron transfer and recombination in DSCs. Hence, EIS was further performed in the frequency range of 0.01 Hz to 100 kHz. Figure 5 shows the

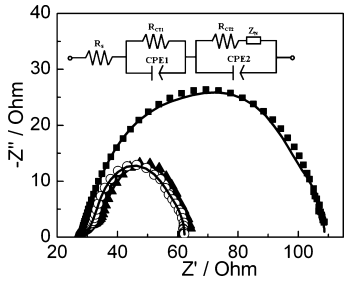

Figure 5. Nyquist plots for EIS of DSCs with the as-prepared photoanodes (solid squares), the sintered photoanodes (solid triangles) and the pressed photoanodes (open circles); the solid lines are the fitting results according to the equivalent circuit shown in the inset of the Figure.

Nyquist plots of DSCs with three kinds of EPD electrodes at forward bias of the open-circuit voltage under illumination of 100 mW cm^{-2}. Generally, three characteristic semicircles can be obtained from EIS spectra according to the EIS model reported in the literature.[9,23,24] The small semicircle at high frequency (in the kHz range) is ascribed to the charge transfer process at the interfaces between the electrolyte and the platinized counter electrode. The large semicircle at the lower frequency (in the 10−100 Hz range) is related to the transport process of the injected electrons within TiO_2 porous films and the charge transfer process of the injected electrons at the interfaces between TiO_2 and the electrolyte. The small feature (in the mHz range) is attributed mainly to the Nernst diffusion of I_3^- within the electrolyte. As can be seen, the typical semicircles in the Nyqusit plot for as-deposited electrode are overlapped together, showing a semicircle in the middle frequency. This is mainly due to presence of micro cracks that lead to the poor connection between the TiO_2 particles and the substrate.[24] After post-treatment on the as-prepared film, two characteristic semicircles are presented. The semicircle at high frequency can be ascribed to the charge transfer at the interfaces of the electrolyte/Pt counter electrode, and the other at the low frequency is related to the accumulation/transport of the injected electrons with TiO_2 porous film and the charge transfer at the electrolyte/TiO_2 interfaces, respectively. The arc related to the diffusion of I_3^- is not observed and overlapped due to the low viscosity of the liquid electrolyte and short length for I_3^- ion diffusion caused by the thin space used in the study. The semicircle size of the middle frequency region in devices based on sintered and pressed films decreases compared to DSC with as-prepared film, because of the acceleration of electron transfer process in the photoanode. The impedance spectra were analyzed by Z-view software using an equivalent circuit containing constant phase (CPE) elements and resistances (R) shown in the inset of Figure.5.[9,24] The fitting values of R_{ct2} for as-prepared electrode, sintered and pressed TiO_2 electrode are 82.2, 28.6, and 20.4 ohm, respectively. It confirms that the R_{ct2} decreases dramatically after post-treatment, especially by compression. The decrease in R_{ct2} can lead to enhancement of collection for photo-generated electrons from TiO_2 surface to conducting substrate after post treatment, resulting in increase of J_{sc}.[36,37] The decrease in R_{ct2} with post-treatment is consistent with the corresponding increase in J_{sc}. And the low transfer resistance could be an important factor for the improvement of the photovoltaic performance of the device with different post-treatments.

As-mentioned above, EPD combined with compression is an effective method to fabricate high performance photoanodes at room temperature. In addition, the thickness of TiO_2 film can be tuned by adjusting the deposition time. Figure 6 shows the

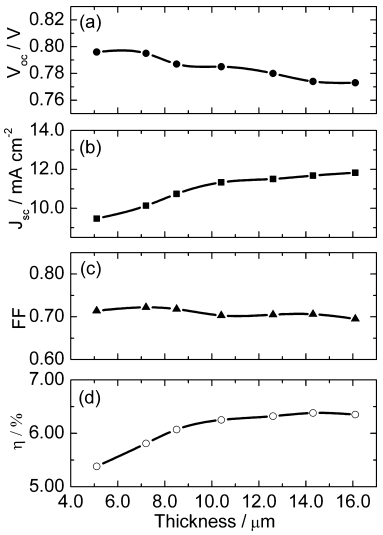

Figure 6. Photovoltaic characteristics of D149-sensitized P25 TiO_2 solar cells as a function of film thickness (AM 1.5G, 100 mW cm^{-2}).

photovoltaic characteristics of D149-sensitized P25 TiO_2 solar cells as a function of film thickness on rigid glass substrates. The V_{oc} (Figure.6a) decreases slightly from 0.796 to 0.772 V with the increasing film thickness from 5.1 to 16.1 μm, which can be attributed to the larger amount of defects and recombination for the thicker films.[20a,22] The J_{sc} (Figure.6b) increases from 9.47 to 11.85 mA cm^{-2} with the increased film thickness, which is due to the increased dye loading. Similar results were also observed for DSCs based on P25 TiO_2 film prepared by high temperature sintering.[38] The FF (Figure 6c) changes slightly between 0.722 and 0.695 due to higher series resistance for the thicker film. Finally, the highest overall efficiency shows a peak value of 6.38% at the film thickness of 14.3 μm with a V_{oc} of 0.774 V, a J_{sc} of 11.68 mA cm^{-2}, and a FF of 0.706 (Figure 6d).

The use of a scattering layer to better utilize the incident light is a well-known strategy to increase device efficiency.[20a,39] Using an identical deposition method, a 1.4 μm layer of 400 nm TiO_2 was subsequently deposited as a scattering layer. The photocurrent−voltage curve of the corresponding DSC is

shown in Figure 7 (open circles). The efficiency of the device fabricated at room temperature reached 7.05% with a V_{oc} of

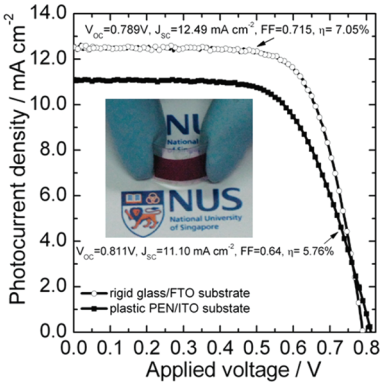

Figure 7. Current density–voltage characteristics curves of D149-sensitized P25 TiO_2 solar cells on rigid glass-FTO substrate (open circles) and on plastic PEN-ITO substrate (solid circles), measured under illumination of 100 mW cm^{-2}, AM1.5G.; insert shows the plastic D149-sensitized P25 electrode.

0.789 V, a J_{sc} of 12.49 mA cm^{-2}, and a FF of 0.715, which is comparable to the DSCs fabricated with P25 using EPD and conventional high temperature sintering.[38]

Plastic DSCs on PEN/ITO substrates were fabricated using the similar conditions for rigid DSCs. Plastic Pt counter electrodes were fabricated by sputtering.[20a] The corresponding photocurrent–voltage curve is also shown in Figure 7 (solid circles). The corresponding photovoltaic parameters are 0.811 V (V_{oc}), 11.10 mA cm^{-2} (J_{sc}), 0.640 (FF), and 5.76% (η), respectively. The efficiency of plastic device is lower than that of rigid glass device resulting from the decrease in J_{sc} and FF, which is largely due to the low transmittance of light for PEN-ITO substrate, and high resistance of the Pt/PEN-ITO electrode.[37] The application of UV–O_3 treatment and antireflection film on plastic substrate is expected to further improve the device performance.[26]

4. CONCLUSION

In conclusion, we report high performance plastic DSCs with low-cost commercial P25 TiO_2 as the photoanode material and with D149 as the dye sensitizer. The results of IMPS, IPCE and EIS reveal that as for the as-prepared electrode via EPD, the compression post-treatment is more efficient than sintered-treatment in improving interfacial connection, interparticle connectivity, photocurrent density and power conversion efficiency of device. The improved performance is ascribed to the enhanced electron transport in the film and charge collection efficiency in the substrate. Full plastic DSC based on P25 TiO_2 with conversion efficiency of 5.76% (AM 1.5G, 100 mW cm^{-2}) were obtained using EPD method combined with compression at room temperature. In addition, the fabrication process was completed within a few hours. This is beneficial to eliminating the fabrication costs, and is thus ideal for low-cost plastic DSCs.

■ ASSOCIATED CONTENT

Supporting Information

XRD patterns for the as-prepared, sintered, and pressed electrodes, and the dependency of photovoltaic performance on the compression pressure. This material is available free of charge via the Internet at http://pubs.acs.org.

■ AUTHOR INFORMATION

Corresponding Author

*E-mail: cheliub@nus.edu.sg. Fax: +65 6779 1936. Tel: +65 6516 8049.

Notes

The authors declare no competing financial interest.

■ ACKNOWLEDGMENTS

The authors are grateful to the National Research Foundation of Singapore (NRF-279-000-276-272), L'Oreal-Singapore Women for Science National Fellowship 2011, and the National Natural Science Foundation of China (21103032) for financial support.

■ REFERENCES

(1) O'Regan, B.; Grätzel, M. *Nature* **1991**, *353*, 737–740.
(2) Grätzel, M. *Acc. Chem. Res.* **2009**, *42*, 1788–1798.
(3) Yella, A.; Lee, H.-W.; Tsao, H. N.; Yi, C.; Chandiran, A. K.; Nazeeruddin, Md. K.; Diau, E. W.-G.; Yeh, C.-Y.; Zakeeruddin, S. M.; Grätzel, M. *Science* **2011**, *334*, 629–634.
(4) (a) Gao, F.; Wang, Y.; Shi, D.; Zhang, J.; Wang, M. K.; Jing, X. Y.; Humphry-Baker, R.; Wang, P.; Zakeeruddin, S. M.; Grätzel, M. *J. Am. Chem. Soc.* **2008**, *130*, 10720–10728. (b) Liang, M.; Xu, W.; Cai, F. S.; Chen, P. Q.; Peng, B.; Chen, J.; Li, Z. M. *J. Phys. Chem. C* **2007**, *111*, 4465–4472.
(5) (a) Horiuchi, T.; Miura, H.; Sumioka, K.; Uchida, S. *J. Am. Chem. Soc.* **2004**, *126*, 12218–12219. (b) Zhu, W. H.; Wu, Y. Z.; Wang, S. T.; Li, W. Q.; Li, X.; Chen, J.; Wang, Z. S.; Tian, H. *Adv. Funct. Mater.* **2011**, *21*, 756–763. (c) Cui, Y.; Wu, Y. Z.; Lu, X. F.; Zhang, X.; Zhou, G.; Miapeh, F. B.; Zhu, W. H.; Wang, Z. S. *Chem. Mater.* **2011**, *23*, 4394–4401.
(6) Zhang, Q. F.; Cao, G. H. *Nano Today* **2011**, *6*, 91–109.
(7) Yun, J.-H.; Ng, Y.; Ye, C.; Mozer, A. J.; Wallace, G. G.; Amal, R. *ACS Appl. Mater. Interfaces* **2011**, *3*, 1585–1593.
(8) Veerappan, G.; Bojan, K.; Rhee, S.-W. *ACS Appl. Mater. Interfaces* **2011**, *3*, 857–862.
(9) Sun, H. C.; Luo, Y. H.; Zhang, Y. D.; Li, D. M.; Yu, Z. X.; Li, K. X.; Meng, Q. B. *J. Phys. Chem. C* **2010**, *114*, 11673–11679.
(10) Chen, X. B.; Mao, S. S. *Chem. Rev.* **2007**, *107*, 2891–2959.
(11) LindstrÖm, H.; Holmberg, A.; Magnusson, E.; Lindquist, S.-T.; Malmqvist, L.; Hagfeld, A. *Nano Lett.* **2001**, *2*, 97–100.
(12) Zhang, D. S.; Yoshida, T.; Oekermann, T.; Furuta, K.; Minoura, H. *Adv. Funct. Mater.* **2006**, *16*, 1228–1234.
(13) Zhang, D. S.; Downing, J. A.; Knorr, F. J.; McHale, J. L. *J. Phys. Chem. B* **2006**, *110*, 21890–21898.
(14) Durr, M.; Schmid, A.; Obermaier, M.; Rosselli, S.; Yasuda, A.; Nelles, G. *Nat. Mater.* **2005**, *4*, 607–611.
(15) (a) Soeda, K.; Kosugi, D.; Kado, T.; Hayase, S. *Chem. Lett.* **2005**, *34*, 650–651. (b) Tebby, Z.; Babot, O.; Michau, D.; Hirsch, L.; Carlos, L.; Toupance, T. *J. Photochem. Photobiol., A* **2009**, *205*, 70–76. (c) Tebby, Z.; Uddin, T.; Nicolas, Y.; Olivier, C.; Toupance, T.; Labrugère, C.; Hirsch, L. *ACS Appl. Mater. Interfaces* **2011**, *3*, 1485–1491.
(16) Yamaguchi, T.; Tobe, N.; Matsumoto, D.; Arakawa, H. *Chem. Commun.* **2007**, *45*, 4767–4769.
(17) Li, X.; Lin, H.; Li, J. B.; Wang, N.; Lin, C. F.; Zhang, L. Z. *J. Photochem. Photobiol., A* **2008**, *195*, 247–253.
(18) Halme, J.; Saarinen, J.; Lund, P. *Sol. Energy Mater. Sol. Cells* **2006**, *90*, 887–899.
(19) (a) Grinis, L.; Dor, S.; Ofir, A.; Zaban, A. *J. Photochem. Photobiol. A: Chem.* **2008**, *198*, 52–59. (b) Grinis, L.; Dor, S.; Ofir, A.; Zaban, A. *Adv. Funct. Mater.* **2010**, *20*, 282–288.

(20) (a) Yin, X.; Liu, X. Z.; Wang, L.; Liu, B. *Electrochem. Commun.* **2010**, *12*, 1241−1244. (b) Yin, X.; Xue, Z. S.; Liu, B. *J. Power Sources* **2011**, *19*, 62422−2426.
(21) Chen, H.-W.; Hsu, C.-Y.; Chen, J.-G.; Lee, K.-M.; Wang, C.-C.; Huang, K.-C.; Ho, K.-C. *J. Power Sources* **2010**, *195*, 6225−6231.
(22) Ito, S.; Zakeeruddin, S. M.; Humphry-Baker, R.; Liska, P.; Charvet, R.; Comte, P.; Nazeeruddin, M. K.; Péchy, P.; Takata, M.; Miura, H.; Uchida, S.; Grätzel, M. *Adv. Mater.* **2006**, *18*, 1202−1205.
(23) Wang, Q.; Moser, J.-E.; Grätzel, M. *J. Phys. Chem. B* **2005**, *109*, 14945−14953.
(24) Lin, L.-Y.; Nien, P.-C.; Lee, C.-P.; Tsai, K.-W.; Yeh, M.-H.; Vittal, R.; Ho, K.-C. *J. Phys. Chem. C* **2010**, *114*, 21808−21815.
(25) Lin, C. K.; Yang, T. J.; Feng, Y. C.; Tsung, T. T.; Sue, C. Y. *Surf. Coat. Technol.* **2006**, *200*, 3184−3189.
(26) Yamaguchi, T.; Tobe, N.; Matsumoto, D.; Nagai, T.; Arakawa, H. *Sol. Energy Mater. Sol. Cells* **2010**, *94*, 812−816.
(27) Zhang, Y.; Xie, Z. B.; Wang, J. *ACS Appl. Mater. Interfaces* **2009**, *1*, 2789−2795.
(28) Agarwala, S.; Kevin, M.; Wong, A. S. W.; Peh, C. K. N.; Thavasi, V.; Ho, G. W. *ACS Appl. Mater. Interfaces* **2010**, *2*, 1844−1850.
(29) (a) Yin, X.; Zhao, H.; Chen, L. P.; Tan, W. W.; Zhang, J. B.; Weng, Y. X.; Shuai, Z. G.; Xiao, X. R.; Zhou, X. W.; Li, X. P.; Lin, Y. *Surf. Interface Anal.* **2007**, *39*, 809−816. (b) Yin, X.; Tan, W.; Zhang, J.; Weng, Y.; Xiao, X.; Zhou, X.; Li, X.; Lin, Y. *Colloids Surf., A* **2008**, *326*, 42−47.
(30) Xia, J.; Masaki, N.; Jiang, K.; Yanagida, S. *J. Phys. Chem. B* **2006**, *110*, 25222−25228.
(31) Hwang, D.; Jo, S. M.; Kim, D. Y.; Amerl, V.; MacFarlane, D. R.; Jang, S.-Y. *ACS Appl. Mater. Interfaces* **2011**, *3*, 1521−1527.
(32) Tan, W. W.; Yin, X.; Zhou, X. W.; Zhang, J. B.; Xiao, X. R.; Lin, Y. *Electrochim. Acta* **2009**, *54*, 4467−4472.
(33) Krüger, J.; Plass, R.; Grätzel, M.; Cameron, P. J.; Peter, L. M. *J. Phys. Chem. B* **2003**, *10*, 77536−7539.
(34) Nazeeruddin, M. K.; Kay, A.; Rodicio, I.; Humphry-Baker, R.; Mueller, E.; Liska, P.; Vlachopoulos, N.; Grätzel, M. *J. Am. Chem. Soc.* **1993**, *115*, 6382−6390.
(35) Yang, W. G.; Wan, F. R.; Chen, Q. W.; Li, J. J.; Xu, D. S. *J. Mater. Chem.* **2010**, *20*, 2870−2876.
(36) Hoshikawa, T.; Yamada, M.; Kikuchi, T.; Eguchi, K. *J. Electrochem. Soc.* **2005**, *152*, E68−E73.
(37) Ito, S.; Ha, N.-L.; Rothenberger, G.; Liska, P.; Comte, P.; Zakeeruddin, S. M.; Péchy, P.; Nazeeruddin, M. K.; Grätzel, M. *Chem. Commun.* **2006**, *38*, 4004−4006.
(38) Chang, H.; Su, H.-T.; Chen, W.-A.; Huang, K.-D.; Chien, S.-H.; Chen, S.-L; Chen, C.-C. *Sol. Energy* **2010**, *84*, 130−136.
(39) Shin, K.; Jun, Y.; Moon, J. H.; Park, J. H. *ACS Appl. Mater. Interfaces* **2010**, *2*, 288−291.